ACS APPLIED MATERIALS & INTERFACES

Research Article

www.acsami.org

Cancer Cell Detection and Therapeutics Using Peroxidase-Active Nanohybrid of Gold Nanoparticle-Loaded Mesoporous Silica-Coated Graphene

Swarup Kumar Maji,[†] Amal Kumar Mandal,[†] Kim Truc Nguyen,[†] Parijat Borah,[†] and Yanli Zhao*[,†,‡]

[†]Division of Chemistry and Biological Chemistry, School of Physical and Mathematical Sciences, Nanyang Technological University, 21 Nanyang Link, 637371, Singapore

[‡]School of Materials Science and Engineering, Nanyang Technological University, 50 Nanyang Avenue, 639798, Singapore

Supporting Information

ABSTRACT: Development of efficient artificial enzymes is an emerging field in nanobiotechnology, since these artificial enzymes could overcome serious disadvantages of natural enzymes. In this work, a new nanostructured hybrid was developed as a mimetic enzyme for in vitro detection and therapeutic treatment of cancer cells. The hybrid (GSF@AuNPs) was prepared by the immobilization of gold nanoparticles (AuNPs) on mesoporous silica-coated nanosized reduced graphene oxide conjugated with folic acid, a cancer cell-targeting ligand. The GSF@AuNPs hybrid showed unprecedented peroxidase-like activity, monitored by catalytic oxidation of a typical peroxidase substrate, 3,3′,5,5′-tetramethylbenzidine (TMB), in the presence of H_2O_2. On basis of this peroxidase activity, the hybrid was utilized as a selective, quantitative, and fast colorimetric detection probe for cancer cells. Finally, the hybrid as a mimetic enzyme was employed for H_2O_2- and ascorbic acid (AA)-mediated therapeutics of cancer cells. In vitro experiments using human cervical cancer cells (HeLa cells) exhibited the formation of reactive oxygen species ($OH^{\bullet}$ radical) in the presence of peroxidase-mimic GSF@AuNPs with either exogenous H_2O_2 or endogenous H_2O_2 generated from AA, leading to an enhanced cytotoxicity to HeLa cells. In the case of normal cells (human embryonic kidney HEK 293 cells), the treatment with the hybrid and H_2O_2 or AA showed no obvious damage, proving selective killing effect of the hybrid to cancer cells.

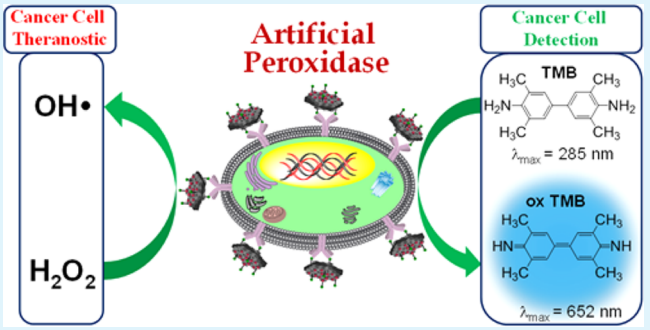

KEYWORDS: *cancer cell detection, gold nanoparticles, graphene, peroxidase activity, therapeutics*

1. INTRODUCTION

Enzymes as biological catalysts involved in almost all reactions in vivo have attracted great interests in pharmaceutical processes, agrochemical production, food industry applications and biosensing, on account of their superior catalytic power and excellent substrate specificity in mild reaction conditions.[1,2] However, their practical applications are largely restricted because of some serious disadvantages, such as low sensitivity of catalytic activity under environmental conditions, low operational stability, and high costs in the preparation and purification.[3,4] To overcome these issues, nanomaterial-based enzyme mimics have been developed, showing significant promises. For instance, Gao et al. discovered intrinsic enzyme-mimetic activity of Fe_3O_4, which was similar to that of natural peroxidases.[4] In the past few years, several types of nanostructured materials have been investigated as artificial enzymes for catalytic oxidation of peroxidase substrates in the presence of hydrogen peroxide (H_2O_2).[5−15] On the basis of this attractive property, these enzyme mimics exhibit potential applications in bioanalysis and environmental detection.[16−18] Although several studies for the design of artificial enzymes have been reported,[4−18] new generation hybrid nanostructures with enhanced catalytic activity, high stability, and less toxicity are still of great interest to replace conventional peroxidase systems for practical applications.

Graphene based materials are attracting special attention in the areas of materials science and biomedicine on account of their extraordinary physiochemical properties originated from unique structure of graphene, including high mechanical strength, large surface area, good biocompatibility, high chemical stability, and acting as suitable platforms for heterogeneous catalytic processes.[19,20] Successful utilization of graphene for biorelated applications, such as biosensing through fluorescence and electrochemistry, graphene-assisted cell imaging, and graphene-based nanocarriers for drug delivery and cancer therapy, has been achieved in the past few years.[19−25] To realize novel functions of graphene based materials and devices for biomedical applications, rational

Received: February 25, 2015
Accepted: April 24, 2015
Published: April 24, 2015

DOI: 10.1021/acsami.5b01758
ACS Appl. Mater. Interfaces 2015, 7, 9807−9816

Scheme 1. Schematic Illustration of Peroxidase Activity of GSF@AuNPs for Cancer Cell Detection and Therapeutic Cancer Treatment

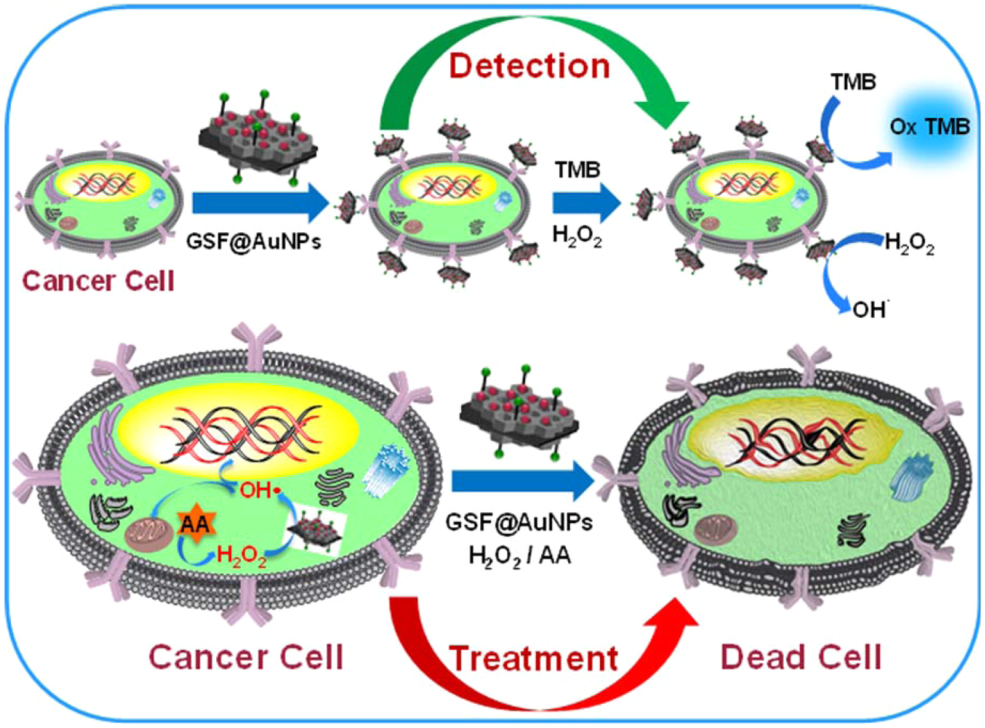

design of graphene based materials is highly required. Thus, the combination of graphene sheets as two-dimensional (2D) building blocks with suitable assemblies to form functional hybrid systems is essential to extend its biomedical applications. Recently, Yang et al. developed a sandwich nanocomposite of graphene oxide (GO) with periodic mesoporous silica (PMS) for effective lithium ion storage and oxygen electrocatalytic reduction.[26] Afterward, the GO-PMS based sandwich hybrid was used for targeted chemo-photothermal therapy of glioma,[27] catalytic oxidation of carbon monoxide, and reduction of 4-nitrophenol,[28] and served as a template for the synthesis of graphene-based carbon nitride nanosheets as metal-free electrocatalysts for oxygen reduction reactions.[29] We and others recently reported silica coated GO-containing noble metal nanoparticles for catalysis[30] and electrochemical biosensing.[31]

On the other hand, intrinsic peroxidase-like activity of graphene has been established in recent years.[21] Till now, various biomolecules, such as glucose,[21] proteins,[32] and specific DNA sequences,[33] have been detected by utilizing the peroxidase activity of GO with the peroxidase substrate, 3,3′,5,5′-tetramethylbenzidine (TMB), in the presence of H_2O_2 to produce a blue colored product. GO has also been employed for targeted cancer cell detection by constructing a hybrid material with hemin through peroxidase activity.[34] But, further kinetic analysis using the hybrid proved a similar catalytic activity to that of hemin.[33] Although some examples demonstrate the potentiality of GO and GO-based nanomaterials as artificial enzymes to replace natural horseradish peroxidase (HRP),[35−40] further investigations to design and fabricate more suitable GO-based hybrids that could be able to provide enhanced catalytic performance are of contemporary interest for a wide range of practical applications.

Herein, we developed a facial approach to fabricate a new generation 2D nanostructured hybrid by immobilizing small gold nanoparticles (AuNPs, ∼5 nm in diameter) on the surface of PMS coated reduced GO (RGO, 100−400 nm in size). Since AuNPs have been reported[11] to show peroxidase-like activity, an enhanced peroxidase performance by rational combination of AuNPs and RGO-PMS was expected. The PMS coating on RGO is to (i) serve as a platform for the stable immobilization of AuNPs on the hybrid surface, (ii) reduce the aggregation of AuNPs for peroxidase application, and (iii) facilitate the conjugation of cancer cell-targeting ligand on the hybrid. Thus, RGO-PMS was further conjugated with cancer cell-targeting ligand, folic acid (FA), to achieve RGO-PMS-FA. After the immobilization of AuNPs, the final hybrid GSF@AuNPs was obtained to serve as a robust nanoprobe for quantitative, selective, and fast colorimetric detection of cancer cells, as well as for therapeutic cancer treatment through superior peroxidase activity of the hybrid (Scheme 1).

2. EXPERIMENTAL SECTION

2.1. General Measurements. Powder X-ray diffraction (XRD) patterns were obtained by Shimadzu XRD-6000 parallel beam X-ray diffractometer with Bragg-Bretano focusing geometry and monochromatic CuKα radiation (λ = 1.540598 Å). Transmission electron microscopy (TEM) analyses were performed on a FEG-TEM (JEM-2100F, JEOL, Japan) operated at 200 kV. X-ray photoelectron spectroscopy (XPS) analyses were performed by SPECS HSA3500 plus spectrometer using Mg X-ray source. Energy dispersive X-ray spectrum (EDS) was collected using a HITACHI S-4500 instrument. Nitrogen adsorption/desorption measurements were carried out by Brunauer−Emmett−Teller (BET) technique using Quantachrome Instruments Autosorb-iQ (Boynton Beach, Florida USA). Fourier transform infrared (FTIR) spectroscopy was performed on a JASCO FTIR-460 plus spectrophotometer with a potassium bromide (KBr) pallet method. Electronic absorption spectra were collected on a Shimadzu UV-3101 PC NIR scanning spectrophotometer. The cell viability and colorimetric assay tests were performed by using a micro

DOI: 10.1021/acsami.5b01758
ACS Appl. Mater. Interfaces 2015, 7, 9807−9816

Scheme 2. Schematic Illustration of Synthetic Procedure for the Preparation of GSF@AuNPs

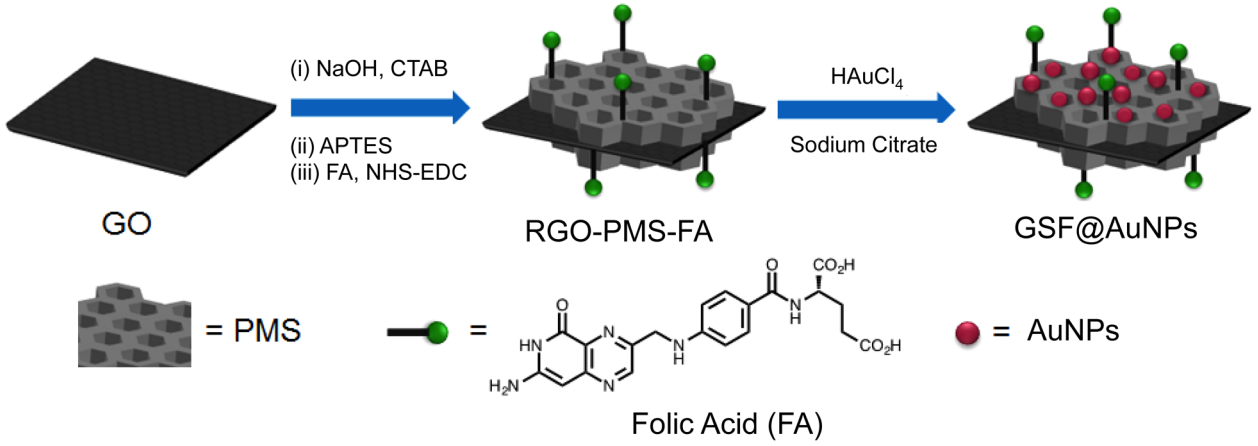

plate reader Infinite 200 PRO, Tecan. The fluorescence images were captured using a Nikon D-Eclipse C1 fluorescence microscope.

2.2. Synthesis of GSF@AuNPs Hybrid. GO was synthesized by a modified Hurmenr's method.[41] Nanosized RGO[21] and sandwich-like coating of PMS on RGO (RGO-PMS) were carried out according to a previous report (see Supporting Information).[26] The introduction of $-NH_2$ group on the RGO-PMS sheets was performed by refluxing ethanolic solution (10 mL) of RGO-PMS (10 mg) with (3-aminopropyl) triethoxysilane (APTES, 100 μL) at 80 °C for 12 h.[31] After cooling down to room temperature, the product (RGO-PMS-NH_2) was collected by centrifugation followed by washing with ethanol. The as-obtained product was transferred into dimethyl sulfoxide (DMSO) solution (20 mL) containing FA active ester (400 mg) that was synthesized according to a previous report.[42] The pH of the solution mixture was adjusted to 8−9 by triethylamine and then stirred at 30−40 °C for 24 h. After the conjugating reaction, the product (RGO-PMS-FA) was collected by centrifugation followed by washing with DMSO and ethanol.

In the final step, AuNPs were in situ immobilized on the surface of RGO-PMS-FA through a commonly used citrate reduction method.[43] RGO-PMS-FA (5 mg) was dispersed in deionized water (5 mL), and mixed with $HAuCl_4$ (500 μL, 10 mM) under continuous stirring for 6 h. The solution mixture was then heated to 100 °C and sodium citrate (1 mL, 0.1 M) was added with stirring for another 1 h. After cooling down to room temperature, the final hybrid material (GSF@AuNPs) was collected by centrifugation and washed with ethanol.

2.3. Peroxidase Activity Measurements. The catalytic experiments were carried out in phosphate buffer solution (PBS, pH 5, 3 mL) containing H_2O_2 (13 mM) and TMB (0.1 mM) in the absence or presence of GSF@AuNPs (45 μg mL^{-1}). The comparative experiments were carried out in PBS containing TMB, along with (i) H_2O_2 in the absence of any catalyst, (ii) nanosized GO and H_2O_2, (iii) GSF@AuNPs in the absence of H_2O_2, and (iv) GSF@AuNPs with H_2O_2 under similar conditions. The kinetic analyses were measured by using GSF@AuNPs (μg mL^{-1}) with (i) a fixed amount of H_2O_2 (13 mM) and different amounts (0−200 μM) of TMB solutions, and (ii) a fixed amount of TMB (0.1 mM) and different amounts (0−81 mM) of H_2O_2. All reactions were monitored by measuring the absorbance at 652 nm. The kinetic parameters were calculated using the Michaelis−Menten model based on the equation $V = V_{max}[S]/(K_m + [S])$, where $[S]$ is the concentration of the substrate, V is the initial velocity, V_{max} is the maximal velocity, and K_m is the Michaelis constant.[10]

2.4. Cell Culture, Colorimetric Detection, and Cell Viability Measurements. Human embryonic kidney cells (HEK 293 normal cells) and human cervical cancer cells (HeLa cells) were grown in Dulbecco's Modified Eagle's Medium (DMEM) cell culture medium containing 10% fetal bovine serum, penicillin (100 U mL^{-1}), and streptomycin (100 mg mL^{-1}) under a humidified atmosphere with 5% CO_2 at 37 °C.

For the colorimetric assay, different numbers of cells were seeded into 96-well plate at 37 °C for 1 day. After it was washed with PBS (10 mM, pH 7.4), the cells were fixed with 4% paraformaldehyde at room temperature for 10 min to disrupt the endocytosis process of the cells. Then, formaldehyde was removed. The cells were again washed with PBS and allowed to incubate with GSF@AuNPs (45 μg mL^{-1}) for 2 h. The cells were washed with PBS to remove unattached GSF@AuNPs. After that, PBS (10 mM, pH 5, 200 μL) containing TMB (0.75 mM) and H_2O_2 (200 mM) was added to each well, and subsequently the absorbance at 652 nm was measured with a micro plate reader.

The cell viability tests were performed by the standard MTT (3-(4,5-dimethylthiazol-2-yl)-2,5-diphenyltetrazolium bromide) assay method. All the cells were seeded into 96-well plate (1×10^4 cells per well) in DMEM cell culture medium. After 12 h, the medium was replaced with fresh DMEM (100 μL per well) and then allowed to incubate with different concentrations of GSF@AuNPs for another 12 h. H_2O_2 (15 or 30 μM) or AA (1 or 2 mM) was added for further 2 h of incubation. The cells were washed with PBS and then cultured for another 18 h. After that, the medium was replaced with DMEM (100 μL per well) containing MTT (0.5 mg mL^{-1}) followed by the incubation for 4 h. The medium was removed and the violet frozen crystals were dissolved with DMSO (100 μL). The absorbance intensity at 565 nm was recorded by a micro plate reader. The relative cell viability (%) of the hybrid to the control well was calculated by $[A]_{test}/[A]_{control}$, where $[A]_{control}$ and $[A]_{test}$ are the average absorbance of the control and test samples, respectively.

For the cell imaging studies, the cells were seeded in 35 mm plastic-bottomed μ-dishes (1×10^5 cells per dish) and grown in DMEM for 1 day. Then, the cells were treated with GSF@AuNPs (45 μg mL^{-1}) for 12 h. After the medium was removed, the cells were washed with PBS and fixed with 4.0% formaldehyde at room temperature. After 10 min, formaldehyde was removed and the cells were again washed with PBS. In the case of H_2O_2 or AA induced cancer cell treatment, after the growth and incubation with GSF@AuNPs for 12 h, H_2O_2 (30 μM) or AA (2 mM) was added with further incubation for 4 h. Then, the cells were washed with PBS and fresh DMEM was added with incubation for another 18 h. The slides were prepared according to a standard protocol. The fluorescence images were captured using a Nikon D-Eclipse C1 fluorescence microscope.

2.5. Terephthalic Acid Photoluminescence Probing Technique. PBS buffer (3 mL, pH 5) containing terephthalic acid (5×10^{-3} M) was subjected to react in the absence or presence of H_2O_2 (5 mM) with different concentrations of GSF@AuNPs (30−60 μg mL^{-1}). The photoluminescence spectra under the excitation wavelength of 315 nm were recorded after 4 min in each case after H_2O_2 addition.

3. RESULTS AND DISCUSSION

3.1. Material Synthesis and Characterization. At first, GO was synthesized and then cut into small pieces to get the

DOI: 10.1021/acsami.5b01758
ACS Appl. Mater. Interfaces 2015, 7, 9807−9816

nanosized GO by reoxidation of GO sheets followed by probe sonication and filtration through syringe filter.[21] The as-synthesized GO sheets were coated with PMS on both sides by hydrothermal treatment in the presence of cetyltrimethylammonium bromide (CTAB) and tetraethyl orthosilicate (TEOS).[26] The obtained RGO-PMS was refluxed with (3-Aminopropyl)triethoxysilane (APTES) to realize -NH_2 functionalized RGO-PMS (RGO-PMS-NH_2). Afterward, FA was conjugated onto RGO-PMS-NH_2 through *N*-hydroxysuccinimide-ethyl(dimethylaminopropyl) carbodiimide (NHS-EDC) coupling reaction between $-NH_2$ and FA activated ester, achieving RGO-PMS-FA.[42] Finally, the desired GSF@AuNPs hybrid was obtained by the reduction of $AuCl_4^-$ through sodium citrate to form small AuNPs over RGO-PMS-FA.[43] The overall synthetic strategy is illustrated in Scheme 2.

UV−vis and FTIR spectroscopic tools were utilized for the initial characterization of the hybrid (Figures S1 and S2 in the Supporting Information). As shown in Supporting Information Figure S1, well resolved characteristic absorption peaks at 234 and 300 nm were observed for nanosized GO,[33] whereas the former peak shifted to 265 nm and the later disappeared after coating with PMS, indicating the formation of RGO.[12] After further conjugation with FA and introduction with AuNPs, the hybrid showed the characteristic peak for FA at 285 nm,[42] and Plasmon absorbance for AuNPs at ∼520 nm.[44] In the FTIR spectra (Figure S2 in the Supporting Information), the formations of RGO-PMS and then RGO-PMS-NH_2 were recognized by the appearance of characteristic bands for symmetric and asymmetric stretching, as well as bond bending vibration of Si−O−Si, and for stretching, bond bending vibration, and plane bending vibration of N−H, respectively.[27] The conjugation of FA to RGO-PMS-NH_2 through the formation of an amide bond between the −COOH group of FA and $-NH_2$ group of RGO-PMS-NH_2 was confirmed by the newly generated peak at 1606 cm^{-1}.[42] The appearance of C═O stretching at 1402 cm^{-1} from citrate group further confirmed the AuNPs deposition on the hybrid.

The morphological characterization was carried out by TEM (Figure 1). The typical TEM image of RGO-PMS revealed the successful growth of PMS on nanosized GO with a size range from 100 to 400 nm (Figure 1a and 1b). The well-oriented PMS in RGO-PMS with an average pore diameter of 3.1 nm could be observed from the high-resolution TEM image (HR-TEM, Figure 1b) and further supported by the BET analysis (Figure S3 in the Supporting Information). RGO-PMS showed high specific surface area of 879.67 $m^2\ g^{-1}$. The TEM images (Figure 1c and 1d) of the GSF@AuNPs hybrid exhibited well-dispersed immobilization of a large number of small AuNPs with an average diameter of 5 nm. The HR-TEM image (inset of Figure 1d) also displayed well-crystalline lattice fringes for AuNPs with interplanar distance of ∼0.235 nm, corresponding to the (111) plane of face center cubic (*fcc*) structure of Au. The AuNPs were only observed on the surface of RGO-PMS sheets, indicating that AuNPs were generated on the sheets not in the solution. As compared with RGO-PMS, a small decrease in the average pore diameter (from 3.1 to 2.9 nm) along with a significant reduction of specific surface area (from 879.67 to 470.87 $m^2\ g^{-1}$) further supported the functionalization and anchoring of AuNPs in the GSF@AuNPs hybrid. Powder XRD pattern of the GSF@AuNPs hybrid clearly showed the peaks for RGO and the *fcc* structure of Au (JCPDS no. 04 0784), suggesting the successful deposition of AuNPs on the surface of RGO-PMS (Figure S4 in the Supporting Information). The

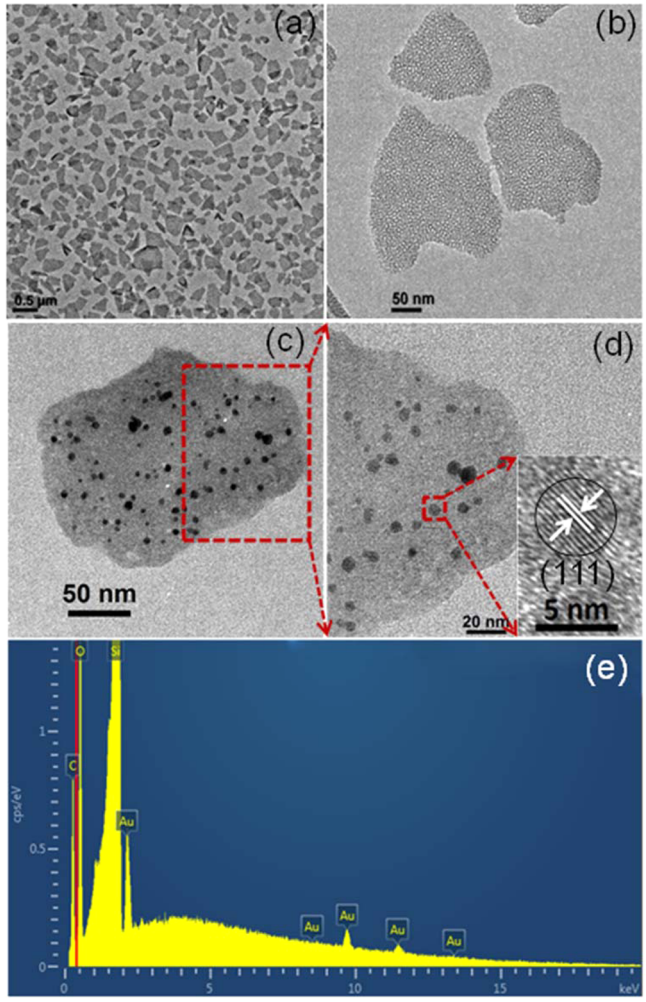

Figure 1. TEM and HR-TEM images of (a, b) RGO-PMS and (c, d) GSF@AuNPs at different magnifications. Inset in Figure d is the HR-TEM image of AuNPs in the hybrid. (e) EDS spectrum of GSF@AuNPs.

average crystal diameter of AuNPs in GSF@AuNPs was calculated to be 4.34 nm by the Scherrer equation, well matching with the TEM analysis.

XPS analysis was also utilized to further characterize the nanostructure of the GSF@AuNPs hybrid. As shown in Figure S5a (Supporting Information), the survey spectrum displayed the existence of all expected elements (C, O, N, Si, and Au) in the hybrid. The high resolution XPS spectrum of C 1s region (Figure S5b in the Supporting Information) showed the presence of C−C bond at 284.4 eV as the major feature, demonstrating the formation of RGO.[33] Two relatively small peaks centered at 285.6 and 286.7 eV were attributed to the C−O and C═O bonds, respectively, further indicating the reduction of GO.[45] Furthermore, the deconvoluted peak centered at 287.7 eV was assigned to the N−C═O bond formed between RGO-PMS-NH_2 and FA, and the peak at 288.9 eV was attributed to the O−C═O bond.[46] Meanwhile, high resolution XPS spectra showed corresponding O 1s and Si 2p regions.[30] In the case of N 1s region, the deconvoluted peaks at 399.13 and 400.03 eV are originated from APTES and FA, respectively.[43] It is interesting to note that the Au $4f_{7/2}$ and Au $4f_{5/2}$ peaks located at 88.0 and 84.4 eV respectively (Figure S 5f in the Supporting Information),[30] again verifying the

DOI: 10.1021/acsami.5b01758
ACS Appl. Mater. Interfaces 2015, 7, 9807−9816

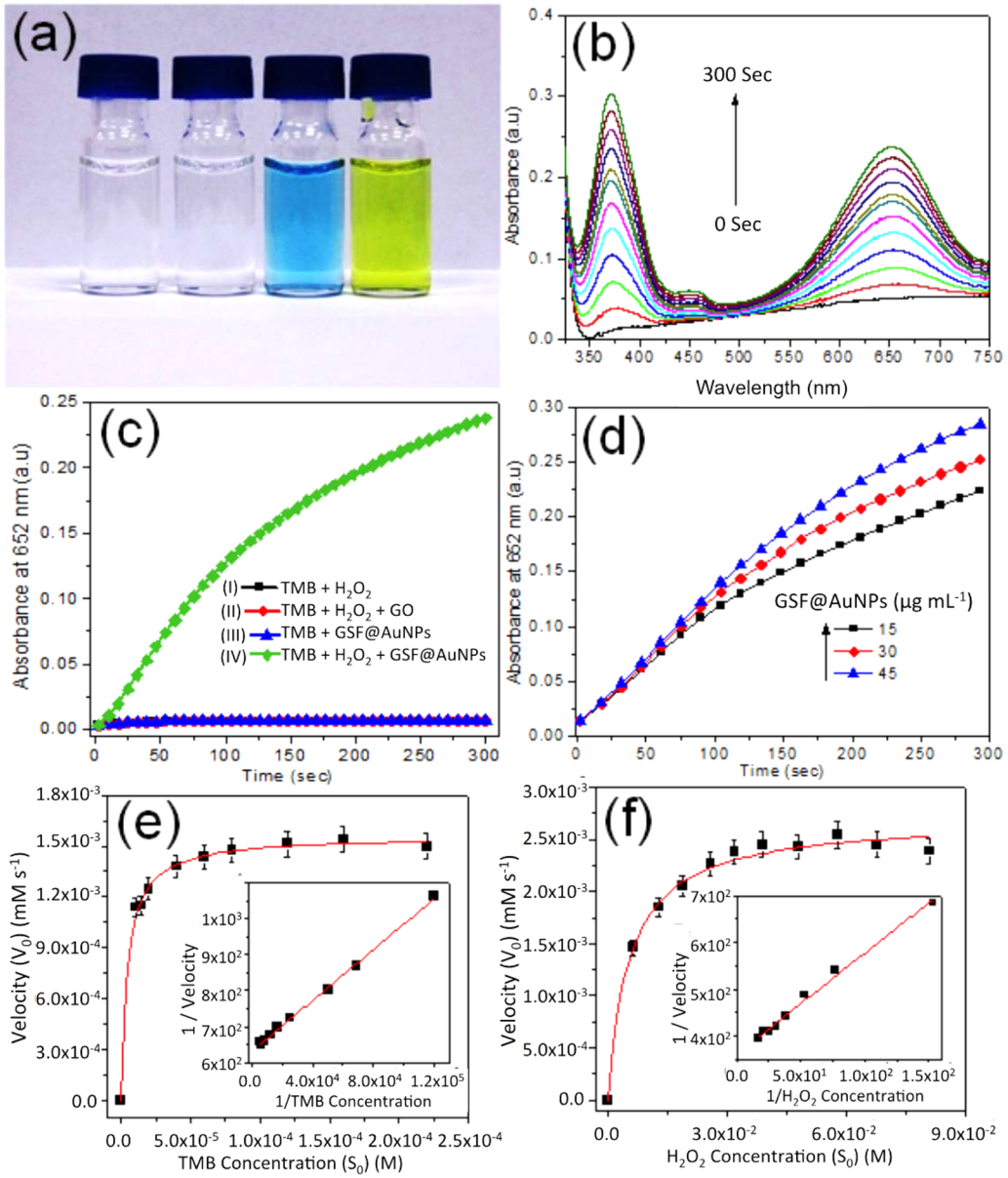

Figure 2. (a) Typical photographs of TMB reaction solution with additions of H_2O_2, GSF@AuNPs, and both GSF@AuNPs and H_2O_2, as well as GSF@AuNPs and H_2O_2 followed by H_2SO_4 for quenched reaction (from left to right). (b) Time-dependent UV−vis spectral changes of TMB solution (0.1 mM) with H_2O_2 (13 mM) catalyzed by GSF@AuNPs (45 μg mL^{-1}). (c) Time-dependent absorbance changes of TMB solution (0.1 mM) at 652 nm in the absence and/or presence of H_2O_2 (13 mM) with GO and GSF@AuNPs. (d) Time-dependent absorbance changes of TMB solution (0.1 mM) with H_2O_2 (13 mM) at 652 nm in the presence of different concentrations of GSF@AuNPs (15−45 μg mL^{-1}). Steady-state kinetic analyses using Michaelis−Menten and Lineweaver−Burk models (insets of figures) for GSF@AuNPs by (e) varying the concentrations of TMB (0−220 μM) with a fixed amount of H_2O_2 (13 mM) and (f) varying the concentrations of H_2O_2 (0−81 mM) with a fixed amount of TMB (0.1 mM).

successful deposition of AuNPs on the surface of RGO-PMS. In addition, the successful anchoring of AuNPs on the surface of RGO-PMS was also established by the corresponding signals in EDS spectrum (Figure 1e). The weight percentage of Au on the hybrid was found to be about ∼2 wt % based on both EDS and XPS analyses.

3.2. Peroxidase Activity of GSF@AuNPs. After successful synthesis and characterization of the GSF@AuNPs hybrid, its intrinsic peroxidase-like activity was examined by the oxidation of a typical peroxidase substrate (TMB) in the presence of H_2O_2, monitored by absorption spectroscopy. In the presence of H_2O_2, GSF@AuNPs could catalyze the oxidation of TMB to ox-TMB with the absorbance maxima at 652 nm, showing the solution color change from colorless to blue (Figure 2a, the third vial). The oxidation could be quenched by H_2SO_4 with the solution color change to yellow (Figure 2a, the fourth vial).[21] It is worthwhile to note that no obvious color change occurred in the absence of GSF@AuNPs (Figure 2a, the first vial) or H_2O_2 (Figure 2a, the second vial), suggesting that both GSF@AuNPs and H_2O_2 are necessary to oxidize TMB. There was no evidence to indicate that the hybrid could also catalyze the oxidation of FA under the same conditions. In the typical absorbance curves for the catalytic reaction (Figure 2b), the absorbance maxima at 370 and 652 nm increased at a time-dependent manner, similar to that of natural enzyme HRP.[21] Comparison experiments were carried out by measuring the

DOI: 10.1021/acsami.5b01758
ACS Appl. Mater. Interfaces 2015, 7, 9807−9816

time-dependent absorbance at 652 nm (Figure 2c) without any catalysts and with GO or GSF@AuNPs to establish the superior catalytic activity of the GSF@AuNPs hybrid under an optimal condition. It was found that the catalytic activity increased upon increasing the added amount of the hybrid to the reaction system (Figure 2d). The significant enhancement of the activity is attributed to the fact that RGO-PMS plays an important role in modulating the catalytic activity of the supported AuNPs.[28] RGO-PMS could be able to provide large specific surface area to increase the loading capacity of TMB on the hybrid through $\pi-\pi$ stacking interactions, while small AuNPs are the responsible species for the catalytic reaction.[28,35] In addition, RGO-PMS acts as a good platform for successful growth of well-dispersed small AuNPs without serious aggregation, thus preserving high catalytic performance of AuNPs.[30] Furthermore, the good stability and reproducibility of the GSF@AuNPs hybrid for the catalytic oxidation of TMB were established by the reuse of the hybrid for five successive measurements (Figure S6 in the Supporting Information).

The steady state kinetics investigated by initial rate method was adopted to determine the kinetic parameters for better understanding the peroxidase activity of the GSF@AuNPs hybrid. As shown in Figure 2e and 2f, typical Michaelis–Menten curves were obtained for the oxidation reaction within a certain concentration range of TMB and H_2O_2. The kinetic parameters could be determined by fitting with Michaelis–Menten model (Figure 2e and 2f) and further validated by Lineweaver–Burk model (insets of Figure 2e and 2f).[4] The measurement of enzyme affinity toward its substrate was determined by the apparent Michaelis–Menten constant (K_m) along with maximal reaction velocity (V_{max}). As listed in Table 1, in comparison with natural enzyme HRP,[4] significantly lower

Table 1. Kinetic Parameters of GSF@AuNPs and HRP Obtained from Their Corresponding Michaelis–Menten Curves

catalyst	substrate	K_m (mM)	V_{max} ($\times 10^{-7}$ M s^{-1})
GSF@AuNPs	TMB	0.005	15.7
	H_2O_2	5.980	27.7
HRP[a]	TMB	0.434	1.00
	H_2O_2	3.700	0.87

[a]Refers to ref 4.

K_m value for the GSF@AuNPs hybrid indicates its better substrate affinity to TMB. The significantly lower K_m value may be attributed to the synergistic effects from RGO-PMS and AuNPs. The PMS coating plays an important role by providing high surface-to-volume ratio and high affinity to TMB for the catalytic oxidation. In addition, good stability of the hybrid by preventing the aggregation leads to higher catalytic activity, that is, lower K_m value. It is also interesting to note that the K_m value of GSF@AuNPs with the TMB substrate is significantly lower than recently reported nanomimics,[5−12] for example, ~30 times smaller than that of GO-AuNCs hybrid.[35] Moreover, the K_m value of GSF@AuNPs with the H_2O_2 substrate is significantly higher than that of HRP, suggesting that higher H_2O_2 concentration is required to achieve the maximal activity of the hybrid.[4] Similar to natural enzymes, higher catalytic efficiency could be attributed to higher ability to bring substrates to the active sites for carrying out the reaction.[4]

3.3. Colorimetric Detection of Cancer Cells. Afterward, the target-directed colorimetric detection of cancer cells based on the superior peroxidase activity of GSF@AuNPs was explored. As above-mentioned, we designed the hybrid material in such a way that it could selectively target cancerous cells through attached FA targeting ligand.[35] Herein, we chose HeLa cell line (human cervical cancer cells) overexpressing folate receptors on the cell membrane, and a normal cell line HEK 293 (human embryonic kidney cells) with lack of folate receptors as a control.[40] At first, the selectivity experiment was carried out by monitoring the blue color generation from the TMB-H_2O_2 solution catalyzed by GSF@AuNPs using two types of cell lines in buffer medium at pH 5. The two cell lines were grown at 37 °C for 1 day and then incubated with GSF@AuNPs (45 μg mL^{-1}) for 2 h. In the cancer cell detection process, the addition of paraformaldehyde disrupted the endocytosis process of the cells, and thus GSF@AuNPs were only adsorbed on the surface of the cells. After the addition of PBS (pH 5) containing TMB-H_2O_2 solution, the specific generation of blue color was observed in the case of HeLa cells (Figure 3a, the third vial), whereas for the wells containing HEK 293 cell (Figure 3a, the second vial) and buffer medium without any cell lines (Figure 3a, the first vial), no significant color change was observed. Thus, the hybrid showed much stronger binding to HeLa cells (~2.5 times) than HEK 293 cells (Figure 3b), confirming its specificity to cancer cells. To further evaluate the capability of the hybrid as a colorimetric assay for quantitative determination of different numbers of cancer cells, an optimized amount of GSF@AuNPs (45 μg mL^{-1}) was incubated with various concentrations of HeLa cells in a 96 well plate. Figure 3c shows the time-dependent absorbance changes at 652 nm in the presence of varying amounts of HeLa cells with the addition of TMB and H_2O_2. In addition, Figure 3d clearly indicates that the reaction system presents gradational blue color evolution with 6 times of increase in absorbance upon increasing the cell number from 50 to 100 000. The color changes could also be visualized by the naked eye. The assay was quite sensitive to cancer cells, and as low as 50 cells could easily be detected, which is lower than that of previously reported GO related materials.[34,35,37] Therefore, the GSF@AuNPs hybrid could be considered as a robust and efficient signaling probe for rapid, accurate, and sensitive detection of cancer cells.

3.4. Therapeutic Treatment of Cancer Cells. Among all the commonly used methods in the cancer treatment, a mild therapeutic strategy, known as oxidative stress, has been widely adopted.[47] It is well know that by activating the oxidative stress, vigorous and excessive reactive oxygen species (ROS) is produced, which causes the damage of cancer cells.[48] On the other hand, due to the antioxidant capacity, normal cells have the capability to tolerate a certain level of exogenous ROS stress.[49] In this research, in addition to the cancer cell detection capability, the GSF@AuNPs hybrid could also be utilized for the therapeutic treatment of cancer cells on account of its efficient generation of $OH^{\bullet}$ radical through the peroxidase activity. The excessive generation of the $OH^{\bullet}$ radical from H_2O_2 catalyzed by GSF@AuNPs was confirmed by the terephthalic acid photoluminescence probing technique.[9] It has been well established that, in the presence of short-lived $OH^{\bullet}$ radical, nonfluorescent terephthalic acid would be converted to a strong fluorescent molecule 2-hydroxylterephthalic acid (HTA) with the maximum emission at 435 nm.[9] As shown in Figure S7 (Supporting Information), the PBS solution (pH 5) of terephthalic acid displayed the absence of any characteristic peak for HTA, while it showed a weak

DOI: 10.1021/acsami.5b01758
ACS Appl. Mater. Interfaces 2015, 7, 9807−9816

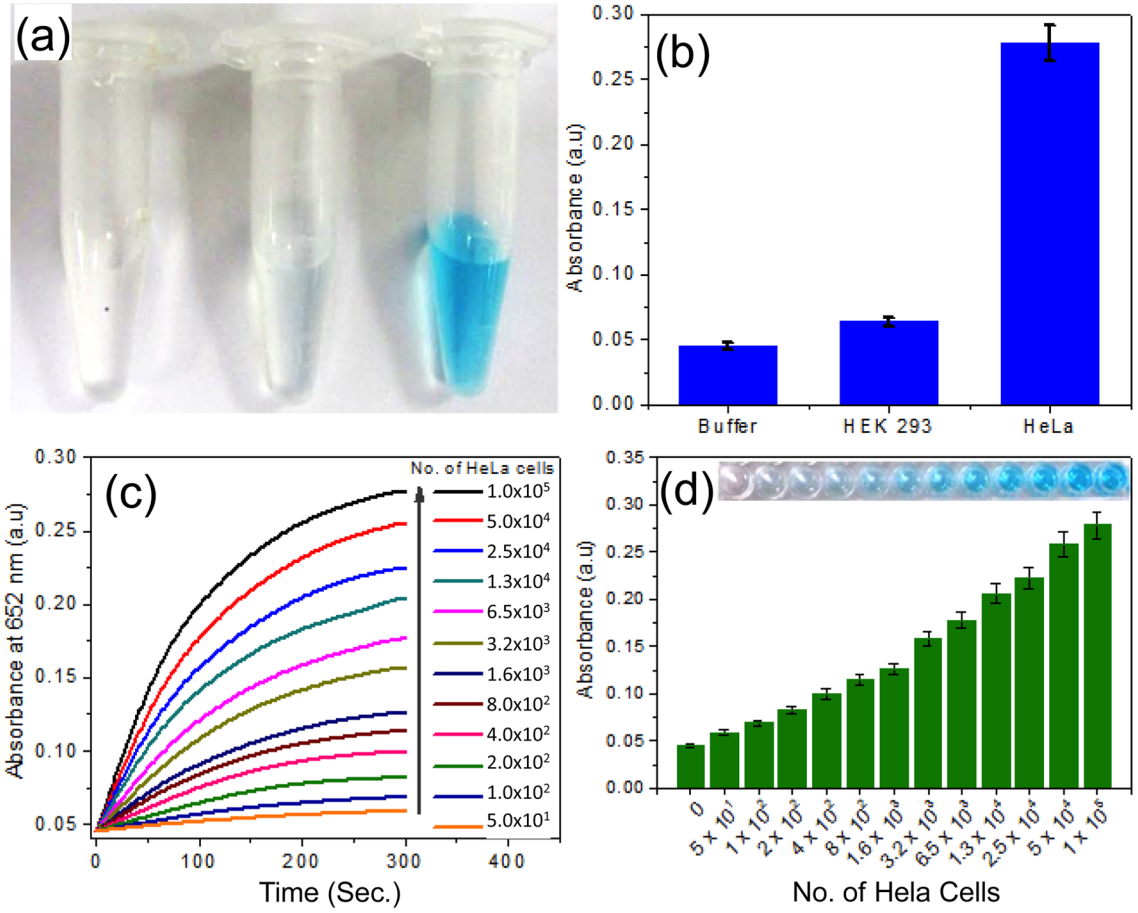

Figure 3. (a) Typical photographs for cancer cell detection using the colorimetric method developed from GSF@AuNPs. From left to right: buffer, HEK 293 cells, and HeLa cells. (b) Target-directed cancer cell detection using GSF@AuNPs indicated by the changes of absorption peak at 652 nm after 300 s. From left to right: buffer, HEK 293 cells (1×10^5), and HeLa cells (1×10^5). (c) Time-dependent absorbance changes at 652 nm upon analyzing different numbers of HeLa cells. (d) The absorption intensity changes at 652 nm after 300 s with different numbers ($0–1 \times 10^5$) of HeLa cells. Inset figures are corresponding photographs of the well plates.

emission peak at 435 nm in the presence of H_2O_2. A drastic enhancement in the emission intensity was observed in the presence of the GSF@AuNPs hybrid in a concentration-dependent manner (Figure S7 in the Supporting Information). This observation indicates that the GSF@AuNPs hybrid is capable of carrying out the catalytic conversion from H_2O_2 to $OH^•$ radical in a concentration-dependent fashion through peroxidase-like behavior, which is similar to that of iron oxide.[4]

GSF@AuNPs was found to possess superior peroxidase activity in acidic pH, which could be related to its anticancer activity by the generation of $OH^•$ radical in cancer cells when taking up into lysosomes. Prior to the anticancer activity of GSF@AuNPs, its inherent toxicity was measured using MTT (3-(4,5-dimethylthiazol-2-yl)-2,5-diphenyltetrazolium bromide) assay, showing a negligible cytotoxicity. To achieve the anticancer activity, different concentrations of GSF@AuNPs (2.81–45 μg mL^{-1}) were incubated with HeLa cells for 12 h. Without using paraformaldehyde, the GSF@AuNPs hybrid was endocytosed by cancer cells under long incubation time (12 h). Then, H_2O_2 (15 or 30 μM) was added into the system, and the system was further incubated for 2 h. The system was washed with PBS and then added with fresh DMEM, followed by further incubation for 18 h. As displayed in Figure 4a, the cell viability markedly decreased in the presence of both GSF@AuNPs and H_2O_2 in a concentration dependent manner. The cell viability decreased up to ~56% after 18 h with 45 μg mL^{-1} GSF@AuNPs and 30 μM H_2O_2, indicating the promising anticancer capability of the hybrid.

Ascorbic acid (AA) is a well-known antioxidant, and for decades it has been used in cancer treatment.[50] According to previous reports, cancer cells can be effectively damaged by the use of pharmacological dosages of AA, in which AA produces endogenous H_2O_2 to result in the oxidative stress by the generation of ROS.[51] In this work, instead of using exogenous H_2O_2, 1 or 2 mM AA was employed along with GSF@AuNPs (2.81–45 μg mL^{-1}) to evaluate the therapeutic efficiency. As shown in Figure 4b, the cell viability decreased dramatically to ~49% in the presence of GSF@AuNPs and 2 mM AA. AA-induced cell viability also showed an obvious concentration-dependent phenomenon for GSF@AuNPs, which is similar to that of exogenous H_2O_2. On the other hand, in the absence of the hybrid, these dosages of AA cannot significantly damage HeLa cells (~84% cell viability), indicating that the endogenous H_2O_2 is probably consumed through multiple metabolism processes. It could be observed that the cell viability (Figure 4c) eventually decreased to ~36% under longer incubation period of 48 h. In order to examine the targeted therapeutic ability of the hybrid to damage only the cancer cells, normal HEK 293 cells were also treated under identical conditions and the cell viability was determined. A negligible cytotoxicity was observed when treated with AA or H_2O_2 alone, and a minor cytotoxicity (~16% cell death at high

DOI: 10.1021/acsami.5b01758
ACS Appl. Mater. Interfaces 2015, 7, 9807–9816

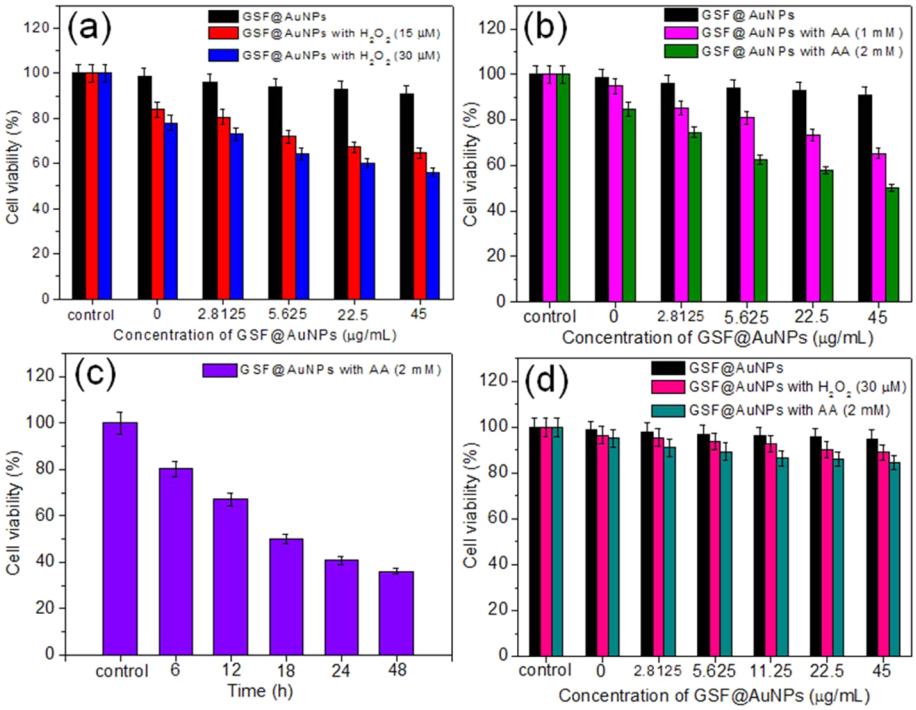

Figure 4. In vitro cell viability tests by MTT assay for HeLa cells in the presence of (a) GSF@AuNPs with H_2O_2 (15 or 30 μM) and (b) GSF@AuNPs with AA (1 or 2 mM). (c) Time-dependent effect of GSF@AuNPs on the viability of HeLa cells in the presence of AA (2 mM). (d) HEK 293 cell viability upon treatment by GSF@AuNPs with H_2O_2 (30 μM) or AA (2 mM).

concentration) was determined for GSF@AuNPs along with H_2O_2 or AA (Figure 4d).

The fluorescence microscopic technique was then applied to visualize the specific targeting ability, as well as the anticancer activity of the hybrid toward HeLa cancer cells. At first, HeLa and HEK 293 cells were grown on a 6-well plate and incubated with GSF@AuNPs (45 μg mL^{-1}) for 4 h. As shown in Figure 5, prominent and clear visualization of green fluorescence was observed for HeLa cells (Figure 5d–f), whereas no significant fluorescence was seen from HEK 293 normal cells (Figure 5a–c), signifying the specific targeting ability of the hybrid to HeLa cancer cells through the FA targeting ligand. Thus, it could be concluded that FA-containing GSF@AuNPs could mainly enter into HeLa cancer cells overexpressed with folate receptor, while the entered amount of GSF@AuNPs into HEK293 normal cells is very less due to the absence of the folate receptor on the normal cells. To visualize the therapeutic efficiency, the cell imaging study was performed on HeLa cells treated by GSF@AuNPs (45 μg mL^{-1}) along with H_2O_2 (30 μM) or AA (2 mM). A visual damage of HeLa cells (dead cells) was clearly observed for both cases (Figure 5g–l), further supporting the finding from the MTT assay. On account of the cancer cell-targeting capability of GSF@AuNPs, the requirement of high concentration of H_2O_2 in cancer cells is not critical. Once GSF@AuNPs are localized within cancer cells, the cancer cells can be further treated with AA to produce endogenous H_2O_2 for peroxidase-based cancer therapy. Therefore, these experimental results demonstrate the excellent capability of the GSF@AuNPs hybrid as a peroxidase mimic for target-directed cancer cell detection, cell imaging, and enhanced generation of ROS, leading to significant damage of specific cancer cells in a time and dosage dependent fashion.

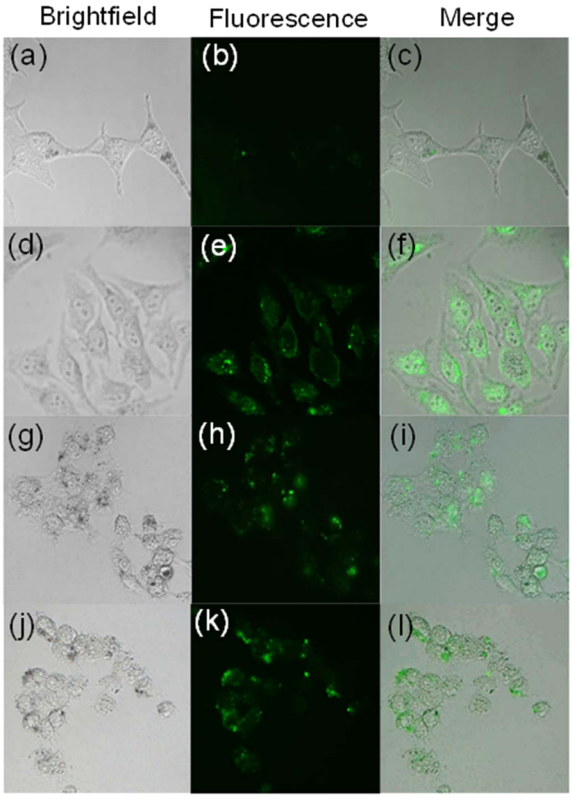

Figure 5. Targeting effect indicated by fluorescence microscopy images of (a–c) HEK 293 normal cells and (d-f) HeLa cancer cells incubated with GSF@AuNPs (45 μg mL^{-1}) for 4 h. Fluorescence microscopy images of HeLa cells incubated with (g–i) GSF@AuNPs with H_2O_2 (30 μM) and (j–l) GSF@AuNPs with AA (2 mM).

DOI: 10.1021/acsami.5b01758
ACS Appl. Mater. Interfaces 2015, 7, 9807–9816

4. CONCLUSION

In summary, a new generation of 2D nanostructured GSF@AuNPs hybrid has been developed by the immobilization of AuNPs onto mesoporous silica coated nanosized RGO conjugated with folic acid. The hybrid exhibits unprecedented intrinsic peroxidase activity with very high substrate-binding affinity as compared to that of HRP and GO supported AuNPs, on account of the synergistic effect from AuNPs and mesoporous silica coated RGO. The superior peroxidase activity of GSF@AuNPs has been utilized for dual applications, that is, (i) selective, quantitative, and rapid colorimetric detection of cancer cells, as well as (ii) cancer therapy by activating oxidative stress. A significant color change has been observed by the oxidation of TMB in the presence of GSF@AuNPs for HeLa cancer cell detection with a detection limit as low as 50 cells, which could be visualized by the naked eye. In the case of therapeutic application, obvious cancer cell damage has been achieved through the enhanced generation of $OH^{\bullet}$ radical from exogenous H_2O_2 mediated by GSF@AuNPs. Instead of directly using exogenous H_2O_2, endogenous H_2O_2 produced by AA inside the cell cytoplasm was also feasible for the enhanced cell cytotoxicity against cancer cells. Both the detection and therapeutic processes are selective to cancer cells, indicating high specificity and robustness of the hybrid. Based on the simple peroxidase behavior, the developed hybrid would be a promising candidate for clinical cancer diagnostics and treatment.

■ ASSOCIATED CONTENT

Ⓢ Supporting Information

Experimental details and additional figures. The Supporting Information is available free of charge on the ACS Publications website at DOI: 10.1021/acsami.5b01758.

■ AUTHOR INFORMATION

Corresponding Author

*E-mail: zhaoyanli@ntu.edu.sg.

Author Contributions

The manuscript was written through contributions of all authors. All authors have given approval to the final version of the manuscript.

Notes

The authors declare no competing financial interest.

■ ACKNOWLEDGMENTS

This research is supported by the National Research Foundation (NRF), Prime Minister's Office, Singapore under its NRF Fellowship (NRF2009NRF-RF001-015) and Campus for Research Excellence and Technological Enterprise (CREATE) Programme, Singapore Peking University Research Centre for a Sustainable Low-Carbon Future, the NTU-A*STAR Silicon Technologies Centre of Excellence under the program grant No. 1123510003, and the NTU-Northwestern Institute for Nanomedicine.

■ REFERENCES

(1) Wolfenden, R.; Snider, M. J. The Depth of Chemical Time and the Power of Enzymes as Catalysts. *Acc. Chem. Res.* **2001**, *34*, 938−945.

(2) Garcia-Viloca, M.; Gao, J.; Karplus, M.; Truhlar, D. G. How Enzymes Work: Analysis by Modern Rate Theory and Computer Simulations. *Science* **2004**, *303*, 186−195.

(3) Xie, J.; Zhang, X.; Wang, H.; Zheng, H.; Huang, Y.; Xie, J. Analytical and Environmental Applications of Nanoparticles as Enzyme Mimetics. *Trends Anal. Chem.* **2012**, *39*, 114−129.

(4) Gao, L.; Zhuang, J.; Nie, L.; Zhang, J.; Zhang, Y.; Gu, N.; Wang, T.; Feng, J.; Yang, D.; Perrett, S.; Yan, X. Intrinsic Peroxidase-Like Activity of Ferromagnetic Nanoparticles. *Nat. Nanotechnol.* **2007**, *2*, 577−583.

(5) Lin, Y.; Ren, J.; Qu, X. Catalytically Active Nanomaterials: A Promising Candidate for Artificial Enzymes. *Acc. Chem. Res.* **2014**, *47*, 1097−1105.

(6) Dai, Z.; Liu, S.; Bao, J.; Ju, H. Nanostructured FeS as a Mimic Peroxidase for Biocatalysis and Biosensing. *Chem.—Eur. J.* **2009**, *15*, 4321−4326.

(7) He, W.; Wu, X.; Liu, J.; Hu, X.; Zhang, K.; Hou, S.; Zhou, W.; Xie, S. Design of AgM Bimetallic Alloy Nanostructures (M = Au, Pd, Pt) with Tunable Morphology and Peroxidase-Like Activity. *Chem. Mater.* **2010**, *22*, 2988−2994.

(8) Mu, J.; Wang, Y.; Zhao, M.; Zhang, L. Intrinsic Peroxidase-Like Activity and Catalase-Like Activity of Co_3O_4 Nanoparticles. *Chem. Commun.* **2012**, *48*, 2540−2542.

(9) Maji, S. K.; Dutta, A. K.; Dutta, S.; Srivastava, D. N.; Paul, P.; Mondal, A.; Adhikary, B. Peroxidase-Like Behavior, Amperometric Biosensing of Hydrogen Peroxide and Photocatalytic Activity by Cadmium Sulfide Nanoparticles. *J. Mol. Catal. A: Chem.* **2012**, *358*, 1−9.

(10) Dutta, A. K.; Maji, S. K.; Srivastava, D. N.; Mondal, A.; Biswas, P.; Paul, P.; Adhikary, B. Synthesis of FeS and FeSe Nanoparticles from a Single Source Precursor: A Study of Their Photocatalytic Activity, Peroxidase-Like Behavior, and Electrochemical Sensing of H_2O_2. *ACS Appl. Mater. Interfaces* **2012**, *4*, 1919−1927.

(11) Wang, S.; Chen, W.; Liu, A.-L.; Hong, L.; Deng, H.−H.; Lin, X.−H. Comparison of the Peroxidase-Like Activity of Unmodified, Amino-Modified, and Citrate-Capped Gold Nanoparticles. *ChemPhysChem* **2012**, *13*, 1199−1204.

(12) Lv, X.; Weng, J. Ternary Composite of Hemin, Gold Nanoparticles and Graphene for Highly Efficient Decomposition of Hydrogen Peroxide. *Sci. Rep.* **2013**, *3*, 3285.

(13) Lin, Y.; Wu, L.; Huang, Y.; Ren, J.; Qu, X. Positional Assembly of Hemin and Gold Nanoparticles in Graphene−Mesoporous Silica Nanohybrids for Tandem Catalysis. *Chem. Sci.* **2015**, *6*, 1272−1276.

(14) Xue, T.; Jiang, S.; Qu, Y.; Su, Q.; Cheng, R.; Dubin, S.; Chiu, C.-Y.; Kaner, R.; Huang, Y.; Duan, X. *Angew. Chem., Int. Ed.* **2012**, *51*, 3822−3825.

(15) Bi, S.; Zhao, T.; Jia, X.; He, P. Magnetic Graphene Oxide-Supported Hemin As Peroxidase Probe for Sensitive Detection of Thiols in Extracts of Cancer Cells. *Biosens. Bioelectron.* **2014**, *57*, 110−116.

(16) Wei, H.; Wang, E. Fe_3O_4 Magnetic Nanoparticles as Peroxidase Mimetics and Their Applications in H_2O_2 and Glucose Detection. *Anal. Chem.* **2008**, *80*, 2250−2254.

(17) Chen, W.; Chen, J.; Feng, Y.−B.; Hong, L.; Chen, Q.-Y.; Wu, L.-F.; Lin, X.-H. Peroxidase-like Activity of Water-Soluble Cupric Oxide Nanoparticles and its Analytical Application for Detection of Hydrogen Peroxide and Glucose. *Analyst* **2012**, *137*, 1706−1712.

(18) Sun, X.; Guo, S.; Chung, C.-S.; Zhu, W.; Sun, S. A Sensitive H_2O_2 Assay Based on Dumbbell-like PtPd-Fe_3O_4 Nanoparticles. *Adv. Mater.* **2013**, *25*, 132−136.

(19) Li, X. L.; Wang, X. R.; Zhang, L.; Lee, S. W.; Dai, H. J. Chemically Derived, Ultrasmooth Graphene Nanoribbon Semiconductors. *Science* **2008**, *319*, 1229−1232.

(20) Zhu, Y. W.; Murali, S.; Cai, W. W.; Li, X. S.; Suk, J. W.; Potts, J. R.; Ruoff, R. S. Graphene and Graphene Oxide: Synthesis, Properties, and Applications. *Adv. Mater.* **2010**, *22*, 3906−3924.

(21) Song, Y. J.; Qu, K. G.; Zhao, C.; Ren, J.; Qu, X. Graphene Oxide: Intrinsic Peroxidase Catalytic Activity and Its Application to Glucose Detection. *Adv. Mater.* **2010**, *22*, 2206−2210.

(22) Liu, Z.; Robinson, T. J.; Sun, X. M.; Dai, H. J. PEGylated Nanographene Oxide for Delivery of Water-Insoluble Cancer Drugs. *J. Am. Chem. Soc.* **2008**, *130*, 10876−10877.

(23) Sreejith, S.; Ma, X.; Zhao, Y. Graphene Oxide Wrapping on Squaraine-Loaded Mesoporous Silica Nanoparticles for Bioimaging. *J. Am. Chem. Soc.* **2012**, *134*, 17346−17349.
(24) Ma, X.; Qu, Q.; Zhao, Y.; Luo, Z.; Zhao, Y.; Ng, K. W.; Zhao, Y. Graphene Oxide Wrapped Gold Nanoparticles for Intracellular Raman Imaging and Drug Delivery. *J. Mater. Chem. B* **2013**, *1*, 6495−6500.
(25) Choi, B. G.; Park, H. S.; Park, T. J.; Yang, M. H.; Kim, J. S.; Jang, S.−Y.; Heo, N. S.; Lee, S. Y.; Kong, J.; Hong, W. H. Solution Chemistry of Self-Assembled Graphene Nanohybrids for High-Performance Flexible Biosensors. *ACS Nano* **2010**, *4*, 2910−2918.
(26) Yang, S.; Feng, X.; Wang, L.; Tang, K.; Maier, J.; Müllen, K. Graphene-Based Nanosheets with a Sandwich Structure. *Angew. Chem., Int. Ed.* **2010**, *49*, 4795−4799.
(27) Wang, Y.; Wang, K.; Zhao, J.; Liu, X.; Bu, J.; Yan, X.; Huang, R. Multifunctional Mesoporous Silica-Coated Graphene Nanosheet used for Chemo-Photothermal Synergistic Targeted Therapy of Glioma. *J. Am. Chem. Soc.* **2013**, *135*, 4799−4804.
(28) Shang, L.; Bian, T.; Zhang, B.; Zhang, D.; Wu, L.-Z.; Tung, C.-H.; Yin, Y.; Zhang, T. Graphene-Supported Ultrafine Metal Nanoparticles Encapsulated by Mesoporous Silica: Robust Catalysts for Oxidation and Reduction Reactions. *Angew. Chem., Int. Ed.* **2014**, *53*, 250−254.
(29) Yang, S.; Feng, X.; Wang, X.; Müllen, K. Graphene-Based Carbon Nitride Nanosheets as Efficient Metal-Free Electrocatalysts for Oxygen Reduction Reactions. *Angew. Chem., Int. Ed.* **2011**, *50*, 5339−5343.
(30) Zhu, C.; Han, L.; Hu, P.; Dong, S. In Situ Loading of Well-Dispersed Gold Nanoparticles on Two-Dimensional Graphene Oxide/SiO_2 Composite Nanosheets and Their Catalytic Properties. *Nanoscale* **2012**, *4*, 1641−1646.
(31) Maji, S. K.; Sreejith, S.; Mandal, A. K.; Ma, X.; Zhao, Y. Immobilizing Gold Nanoparticles in Mesoporous Silica Covered Reduced Graphene Oxide: A Hybrid Material for Cancer Cell Detection through Hydrogen Peroxide Sensing. *ACS Appl. Mater. Interfaces* **2014**, *6*, 13648−13656.
(32) Qu, F. L.; Li, T.; Yang, M. H. Colorimetric Platform for Visual Detection of Cancer Biomarker Based on Intrinsic Peroxidase Activity of Graphene Oxide. *Biosens. Bioelectron.* **2011**, *26*, 3927−3931.
(33) Guo, Y.; Deng, L.; Li, J.; Guo, S.; Wangand, E.; Dong, S. Hemin−Graphene Hybrid Nanosheets with Intrinsic Peroxidase-like Activity for Label-Free Colorimetric Detection of Single-Nucleotide Polymorphism. *ACS Nano* **2011**, *5*, 1282−1290.
(34) Song, Y. J.; Chen, Y.; Feng, L. Y.; Ren, J. S.; Qu, X. G. Selective and Quantitative Cancer Cell Detection Using Target-Directed Functionalized Graphene and Its Synergetic Peroxidase-Like Activity. *Chem. Commun.* **2011**, *47*, 4436−4438.
(35) Tao, Y.; Lin, Y.; Huang, Z.; Ren, J.; Qu, X. Incorporating Graphene Oxide and Gold Nanoclusters: A Synergistic Catalyst with Surprisingly High Peroxidase-Like Activity Over a Broad pH Range and Its Application for Cancer Cell Detection. *Adv. Mater.* **2013**, *25*, 2594−2599.
(36) Kim, M. I.; Kim, M. S.; Woo, M.−A.; Ye, Y.; Kang, K. S.; Lee, J.; Park, H. G. Highly Efficient Colorimetric Detection of Target Cancer Cells Utilizing Superior Catalytic Activity of Graphene Oxide−Magnetic−Platinum Nanohybrids. *Nanoscale* **2014**, *6*, 1529−1536.
(37) Zhang, L.-N.; Deng, H.-H.; Lin, F.-L.; Xu, X.-W.; Weng, S.-H.; Liu, A.-L.; Lin, X.-H.; Xia, X.-H.; Chen, W. In Situ Growth of Porous Platinum Nanoparticles on Graphene Oxide for Colorimetric Detection of Cancer Cells. *Anal. Chem.* **2014**, *86*, 2711−2718.
(38) Ge, S.; Liu, F.; Liu, W.; Yan, M.; Song, X.; Yu, J. Colorimetric Assay of K-562 Cells Based on Folic Acid-Conjugated Porous Bimetallic Pd@Au Nanoparticles for Point-of-Care Testing. *Chem. Commun.* **2014**, *50*, 475−477.
(39) Chen, Z.; Yin, J.−J.; Zhou, Y.−T.; Zhang, Y.; Song, L.; Song, M.; Hu, S.; Gu, N. Dual Enzyme-Like Activities of Iron Oxide Nanoparticles and Their Implication for Diminishing Cytotoxicity. *ACS Nano* **2012**, *6*, 4001−4012.
(40) An, Q.; Sun, C.; Li, D.; Xu, K.; Guo, J.; Wang, C. Peroxidase-Like Activity of Fe3O4@Carbon Nanoparticles Enhances Ascorbic Acid-Induced Oxidative Stress and Selective Damage to PC-3 Prostate Cancer Cells. *ACS Appl. Mater. Interfaces* **2013**, *5*, 13248−13257.
(41) Hummers, W. S.; Offeman, R. E. Preparation of Graphitic Oxide. *J. Am. Chem. Soc.* **1958**, *80*, 1339−1339.
(42) Yang, X.; Wang, Y.; Huang, X.; Ma, Y.; Huang, Y.; Yang, R.; Duana, H.; Chen, Y. Multi-Functionalized Graphene Oxide Based Anticancer Drug-Carrier With Dual-Targeting Function and pH-Sensitivity. *J. Mater. Chem.* **2011**, *21*, 3448−3454.
(43) Ji, X.; Song, X.; Li, J.; Bai, Y.; Yang, W.; Peng, X. Size Control of Gold Nanocrystals in Citrate Reduction: The Third Role of Citrate. *J. Am. Chem. Soc.* **2007**, *129*, 13939−13948.
(44) Abdelhalim, M. A. K.; Mady, M. M.; Ghannam, M. M. Physical Properties of Different Gold Nanoparticles: Ultraviolet-Visible and Fluorescence Measurements. *J. Nanomed. Nanotechol.* **2012**, *3*, No. 1000133.
(45) Hu, Z.; Li, J.; Li, C.; Zhao, S.; Li, N.; Wang, Y.; Wei, F.; Chen, L.; Huang, Y. Folic Acid-Conjugated Graphene−ZnO Nanohybrid for Targeting Photodynamic Therapy under Visible Light Irradiation. *J. Mater. Chem. B* **2013**, *1*, 5003−5013.
(46) Mohapatra, S.; Mallick, S. K.; Maiti, T. K.; Ghosh, S. K.; Pramanik, P. Synthesis of Highly Stable Folic Acid Conjugated Magnetite Nanoparticles for Targeting Cancer Cells. *Nanotechnology* **2007**, *18*, No. 385102.
(47) Zhou, Q.; Liu, L. Z.; Fu, B.; Hu, X.; Shi, X.; Fang, J.; Jiang, B. H. Reactive Oxygen Species Regulate Insulin-Induced VEGF and HIF-1α Expression Through the Activation of p70S6K1 in Human Prostate Cancer Cells. *Carcinogenesis* **2007**, *28*, 28−37.
(48) Perry, G.; Raina, A. K.; Nunomura, A.; Wataya, T.; Sayre, L. M.; Smith, M. A. How Important Is Oxidative Damage? Lessons from Alzheimer's Disease. *Free Radical Biol. Med.* **2000**, *28*, 831−834.
(49) Peer, D.; Karp, J. M.; Hong, S.; Farokhzad, O. C.; Margalit, R.; Langer, R. Nanocarriers as an Emerging Platform for Cancer Therapy. *Nat. Nanotechnol.* **2007**, *2*, 751−760.
(50) Jorissen, W. P.; Belinfante, A. H. The Induced Oxidation of Lactic Acid by Ascorbic Acid and the Cancer Problem. *Science* **1934**, *79*, 13.
(51) Chen, Q.; Espey, M. G.; Sun, A. Y.; Pooput, C.; Kirk, K. L.; Krishna, M. C.; Khosh, D. B.; Drisko, J.; Levine, M. Pharmacologic Doses of Ascorbate Act as a Prooxidant and Decrease Growth of Aggressive Tumor Xenografts in Mice. *Proc. Natl. Acad. Sci. U.S.A.* **2008**, *105*, 11105−11109.

DOI: 10.1021/acsami.5b01758
ACS Appl. Mater. Interfaces 2015, 7, 9807−9816